Irditoxin, a novel covalently linked heterodimeric three-finger toxin with high taxon-specific neurotoxicity

Joanna Pawlak,* Stephen P. Mackessy,[†] Nicole M. Sixberry,[†] Enrico A. Stura,[‡] Marie Hélène Le Du,[‡] Renée Ménez,[‡] Chun Shin Foo,[§] André Ménez,[‡] Selvanayagam Nirthanan,[§] and R. Manjunatha Kini*[,‖,1]

*Department of Biological Sciences, Faculty of Science, National University of Singapore, Singapore; [†]School of Biological Sciences, University of Northern Colorado, Greeley, Colorado, USA; [‡]Département d'Ingénierie et d'Etudes des Protéines, Commissariat à l'Energie Atomique, Gif-sur-Yvette Cedex, France; [§]Neuropharmacology and Lead Discovery Laboratory, National Neuroscience Institute, Singapore; and [‖]Department of Biochemistry and Molecular Biophysics, Medical College of Virginia, Virginia Commonwealth University, Richmond, Virginia, USA

ABSTRACT   A novel heterodimeric three-finger neurotoxin, irditoxin, was isolated from venom of the brown treesnake *Boiga irregularis* (Colubridae). Irditoxin subunit amino acid sequences were determined by Edman degradation and cDNA sequencing. The crystal structure revealed two subunits with a three-finger protein fold, typical for "nonconventional" toxins such as denmotoxin, bucandin, and candoxin. This is the first colubrid three-finger toxin dimer, covalently connected *via* an interchain disulfide bond. Irditoxin showed taxon-specific lethality toward birds and lizards and was nontoxic toward mice. It produced a potent neuromuscular blockade at the avian neuromuscular junction (IC_{50}=10 nM), comparable to α-bungarotoxin, but was three orders of magnitude less effective at the mammalian neuromuscular junction. Covalently linked heterodimeric three-finger toxins found in colubrid venoms constitute a new class of venom peptides, which may be a useful source of new neurobiology probes and therapeutic leads.—Pawlak, J., Mackessy, S. P., Sixberry, N. M., Stura, E. A., Le Du, M. H., Ménez, R., Foo, C. S., Ménez, A., Nirthanan, S., Kini, R. M. Irditoxin, a novel covalently linked heterodimeric three-finger toxin with high taxon-specific neurotoxicity. *FASEB J.* 23, 534–545 (2009)

Key Words: postsynaptic neurotoxin · acetylcholine receptor · neuromuscular junction · snake venom

PEPTIDE TOXINS FROM ANIMAL VENOMS target a variety of physiological processes by binding with remarkable specificity and high affinity to receptors and ion channels. They have played a key role in therapeutic lead discovery and in deciphering the molecular structure and function of receptors and ion channels (1). A classic example of three-finger toxins (3FTXs), which constitute one of the most abundant, nonhomogeneous, and well-documented families of snake venom proteins, is α-bungarotoxin. The 3FTX protein fold is characterized by three β-stranded finger-like loops, emerging from a globular core stabilized by four conserved disulfide bonds. An additional disulfide bridge may sometimes be present in the second (middle) loop, as found in long-chain α-neurotoxins (*e.g.*, α-bungarotoxin) and κ-neurotoxins (*e.g.*, κ-bungarotoxin), or in the first loop, as in nonconventional 3FTXs (*e.g.*, candoxin, bucandin; refs. 2, 3). Nonconventional 3FTXs (4) are generally several orders of magnitude lower in toxicity than classical snake α-neurotoxins. Their molecular targets are largely unknown but presumed to be nicotinic acetylcholine receptor (nAChR) subtypes, because the few examples characterized appear to interact with muscle (α1β1γδ) and neuronal α7 receptors (5, 6).

The overall structural similarity notwithstanding, subtle differences in the three-finger fold, such as in the general morphology of the loops and C-terminal and N-terminal segments (7), enable 3FTXs to recognize diverse molecular targets with precise specificity (8). These targets include the α1 (short-chain and long-chain α-neurotoxins); α7 (long-chain α-neurotoxins) or α2β4 and α3β4 nAChRs (κ-neurotoxins); muscarinic AChRs (muscarinic toxins); L-type calcium channels (calciseptine and FS2 toxin); integrin $α_{IIb}β_3$ (dendroaspins); acetylcholinesterase (fasciculins); phospholipids and glycosphingolipids (cardiotoxins; reviewed in ref. 2); coagulation factor VIIa (hemextin AB complex; ref. 9); and β1/β2-adrenergic receptors (β-cardiotoxin; ref. 10). The structure and function of these molecules, with broad spectrum pharmacology within a highly conserved 3FTX fold, are of great value in the development of novel research tools or in rational drug design.

3FTXs, once believed to exist only in the venoms of elapid snakes, have only recently been found in other nonelapid families (11–15). Currently, almost all known 3FTXs exist as monomers, except for κ-bungarotoxins from *Bungarus* venoms, which are noncovalently linked

homodimers, and the hemextin AB complex from *Hemachatus hemachatus* venom, which is a noncovalently linked hetero-tetramer of two different 3FTX subunits (9). In the present study, we report for the first time a new class of covalently linked heterodimeric 3FTXs purified from the venom of the brown treesnake, *Boiga irregularis*, an invasive colubrid snake introduced on the Pacific island of Guam. This toxin demonstrated potent *in vitro* neurotoxicity specific for the avian neuromuscular junction that accounts for the taxon-specific toxicity of the brown treesnake's crude venom, which is essentially nonlethal to mammals (including humans; refs. 16, 17). Its high resolution crystal structure details the similarities to and significant differences from other known snake 3FTXs, which are essential to understanding and exploiting its novel pharmacology.

MATERIALS AND METHODS

Materials

Glu C endopeptidase was purchased from Wako Pure Chemicals (Osaka, Japan), immobilized TPCK-trypsin was from Pierce Chemical Company (Rockford, IL, USA), Edman degradation reagents were from Applied Biosystems (Foster City, CA, USA), and acetonitrile was from Merck KGaA (Darmstadt, Germany). *Pfu* pyroglutamate aminopeptidase was purchased from Takara Biochemicals (Tokyo, Japan). Ellman's reagent was purchased from Pierce. HPLC columns used included Superdex 30 Hiload (16/60) and μRPC C2/C18 (10 μm 120 Å 2.1×100 mm) from Amersham Pharmacia (Uppsala, Sweden), and Shodex CM-825, Jupiter C_4 and C_{18} (5 μm 300 Å 1×150 mm, 4.6×250 mm and 10 μm 300 Å 10×250 mm) columns were purchased from Phenomenex (Torrance, CA, USA). SDS-PAGE gel standard and silver stain were purchased from Bio-Rad Laboratories (Hercules, CA, USA). RNA isolation (RNeasy mini kit), PCR purification, Qiaquick gel extraction, plasmid miniprep, pDrive cloning, and Hot Start *Taq* Polymerase kits were obtained from Qiagen (Valencia, CA, USA). 3′-Rapid amplification of cDNA end (3′-RACE) kit containing SuperScript II reverse transcriptase was obtained from Invitrogen (Carlsbad, CA, USA). The ABI PRISM BigDye terminator cycle sequencing ready reaction kit was purchased from Applied Biosystems. Gene-specific primers were custom synthesized by 1st Base (Singapore). DNA ladder 1 Kb Plus was purchased from Gibco Life Technologies (Carlsbad, CA, USA). *Eco*RI restriction endonuclease was obtained from New England Biolabs (Beverly, MA, USA). Luria Bertani broth and agar were purchased from Q.BIOgene (Irvine, CA, USA). All other reagents were purchased from Sigma (St. Louis, MO, USA).

Animals

Brown treesnakes (*B. irregularis*) were collected on Guam and imported to Colorado under a permit from the U.S. Fish and Wildlife Service (MA022452-0 to SPM). Snakes were maintained at the University of Northern Colorado Animal Facility (UNC IACUC protocol 9204.1) and were extracted of venom every 2 mo. House geckos (*Hemidactylus frenatus*) were obtained from Bushmaster Reptiles (Longmont, CO, USA). NSA mice were bred in the UNC Animal Facility (UNC IACUC protocol 9401). Twelve- to 16-day-old chickens (*Gallus domesticus*) for *in vivo* toxicity studies were obtained from a local breeder (Greeley, CO, USA). Male Sprague-Dawley rats (250–350 g) were purchased from the Centre for Animal Resources of the National

University of Singapore (Lim Chu Kang, Singapore) and kept in the Animal Research Laboratory of the National Neuroscience Institute (NNI IACUC TNI-07/1/004). Six- to 10-day-old domestic chicks (*G. domesticus*) were purchased from Chew's Agricultural (Lim Chu Kang, Singapore) and delivered on the day of experimentation.

Venom extraction

Extraction of venom was based on an established methodology (18), using 18 μg/g ketamine-HCl and 6.0 μg/g pilocarpine-HCl. Venom was centrifuged for 10 min at 10,000 *g* and was then lyophilized and stored frozen until it was used.

Protein purification

Lyophilized venom (70 mg) was dissolved in 1.0 ml 10 mM HEPES, pH 6.8, containing 100 mM NaCl and 5.0 mM $CaCl_2$, centrifuged to pellet solids, filtered using 0.45 μm syringe tip filters, and subjected to size exclusion chromatography on a 2.8 × 100 cm BioGel P-100 column. Proteins were eluted with the same buffer at 6.0 ml/h at 4°C. Fractions of interest were combined, dialyzed against MilliQ H_2O, and lyophilized. This fraction was reconstituted in 20 mM sodium phosphate buffer, pH 6.8, and subjected to ion-exchange HPLC using a 4.6 × 75 mm Shodex CM-825 column on a Waters HPLC operating under Empower software (flow rate 1.0 ml/min). Final purification was achieved using a Jupiter C_4 RP-HPLC column equilibrated with 0.1% trifluoracetic acid (TFA; v/v) and eluted using a 20–50% linear gradient of acetonitrile (80% in 0.1% TFA); flow rate was 1.0 ml/min. Elution of protein at all steps was monitored at 280 and 220 nm. The purified toxin was then lyophilized and stored frozen until it was used.

Electrophoresis

SDS-PAGE under reducing and nonreducing conditions was carried out on a 15% gel using the Bio-Rad mini-Protean II electrophoresis system. The proteins were visualized by staining with silver stain.

Measurement of free thiol groups

Ellman's reagent (pH 9.0) and toxin solution were combined, the pH of the mixture was adjusted to 8.0 with phosphate buffer, and the absorption was measured at 412 nm after 5 min. Concentrations were calculated by comparison with standards containing known concentrations of reduced glutathione.

Electrospray ionization-mass spectrometry (ESI-MS)

ESI-MS was used to determine the precise mass of the protein fractions. The masses were measured using a Perkin-Elmer Sciex API 300 triple quadrupole LC/MS/MS system (Perkin-Elmer, Wellesley, MA, USA) equipped with an ion-spray interface as described previously (14).

Separation of subunits

Toxin was treated with 20 mM dithiothreitol (DTT) or Tris (2-carboxyethyl)-phosphine hydrochloride (TCEP) for 1 h, and the subunits were separated by RP-HPLC on a 4.6 × 250 mm C_4 column equilibrated with 0.1% TFA (v/v) and eluted using a 20–60% linear gradient of acetonitrile (80% in 0.1% TFA) in 40 min or on a 4.6 × 250 mm C_{18} column with a linear gradient of 30–60% B (60% ACN in 0.1% TFA) in 50 min. The elution of peptides was monitored at 220 and 280 nm.

Total RNA isolation

One *B. irregularis* had venom extracted to stimulate the production of mRNAs in the venom glands and was euthanized by decapitation 4 days postextraction. The venom glands were quickly dissected, placed in RNAlater solution (Qiagen), and kept frozen at $-80°C$ until used. Venom gland tissue (20 mg) was homogenized using a rotor homogenizer, and the total RNA was extracted using an RNeasy mini kit. The amount of RNA was quantified spectrophotometrically at 260 nm.

3′-RACE

cDNA was synthesized from ~1.0 μg of total RNA using SuperScript II reverse transcriptase and 3′-RACE adapter primer [5′-GGCCACGCGTCGACTAGTAC(T)$_{17}$-3′]. The reverse transcription reaction product was treated with RNase H (2 U) for 30 min at 37°C and then used as a template in PCR (95°C, 15 min, hot start; followed by 30 cycles: 94°C, 1 min; 50°C, 1 min; 72°C, 1 min; and final extension at 72°C for 10 min) with sense primer corresponding to the 3FTX signal peptide region (5′-ATGAAACTCTGCTGCTGGCC-3′) and an antisense 3′-RACE abridged universal amplification primer (5′-GGCCACGCGTCGACTAGTAC-3′). The PCR products obtained were visualized using ethidium bromide staining followed by agarose gel (1%) electrophoresis.

Cloning of PCR products

3′-RACE products were purified according to the manufacturer's instructions using a PCR purification kit, ligated with pDrive vector, and transformed into competent *E. coli* cells (DH5α) by heat shock method. Transformants were selected on LB-agar plates containing 100 μg/ml ampicillin and supplemented with isopropyl-β-D-thiogalactopyranosid and 5-bromo-4-chloro-3-indolyl-β-D-galactopyranoside for blue/white colony screening. The sizes of the inserts were estimated by *Eco*RI digestion followed by 1% agarose gel electrophoresis and ethidium bromide visualization.

DNA sequencing

Sequencing reactions were performed using the ABI PRISM BigDye terminator cycle sequencing ready reaction kit. Products resulting from several independent PCRs were sequenced two times in both directions using T7 and SP6 sequencing primers on an ABI PRISM 3100 automated DNA sequencer. cDNA and protein sequences were analyzed using the BLAST program at the National Center for Biotechnology Information web site (www.ncbi.nlm.nih.gov) and ExPASy proteomics tools at www.expasy.ch. Sequences were aligned using the ClustalW program (www.ebi.ac.uk) or DNAMAN version 4.15 (Lynnon Biosoft, Quebec, QC, Canada).

Crystallization

Crystallization experiments were carried out using the sitting drop vapor diffusion method at 291 K (18°C), containing 1 μl of protein and 1 μl of the reservoir solution (for details, see Supplemental Fig. S3). Crystals for data collection were flash-frozen in liquid ethane using a cryoprotectant solution with 25% glycerol added to the crystallization solution. Data were collected on beam line ID-29 at the European Synchrotron Radiation Facility (Grenoble, France).

Structure determination and refinement

Diffraction images were indexed, integrated, and scaled using the HKL2000 package (19). The experimental phasing was performed with the MLPHARE program from CCP4 package (1994) using a MIRAS approach, *i.e.*, the isomorphous signal from the iodine data set was combined with the tungstate anomalous signal. Building of the structure was performed through several cycles of an interactive process, which included map calculation with the program FFT, followed by automated model building using ARP WARP and recalculation of the map, map examination, and manual adjustment of the model with TURBO-FRODO. From a partially built model, phases were calculated using SFALL, and the program SIGMAA was used to combine calculated and experimental phases. Finally, experimental phases were improved with DM (Density Modification) and extended to 1.5 Å. The refinement was performed with Refmac and CNS.

In vivo toxicity test and LD$_{50}$ determination

Lethal toxicity of the purified toxin was determined in three different model animals: NSA mice (*Mus musculus*), domestic chickens (*G. domesticus*), and house geckos (*H. frenatus*). These models were chosen because birds and lizards are typical prey utilized by brown treesnakes. Toxin was dissolved in 0.9% saline, and weight-proportional doses were administered intraperitoneally. Doses were administered to groups of 3 animals/dose: NSA mice, 0–25 μg/g in 100 μl total volume; chickens and lizards, 0–10 μg/g in 100 μl total volume. Periodic observations of effects, survival time and lethality at 24 h were recorded, and lethal toxicity (LD$_{50}$) was calculated for each species. All toxicity assays were conducted in accordance with approved procedures (UNC IACUC protocol 9402).

Chick biventer cervicis muscle (CBCM) preparations

Pairs of CBCMs were isolated as described previously (6, 14) and mounted in a 6 ml organ bath. All experimental setups and recordings were as described previously (6, 14). The effects of various concentrations of IrTx or α-bungarotoxin (0.01–1 μM) were investigated. Neuromuscular blockade are expressed as a percentage of the original twitch height before the addition of toxin. Concentration-response curves represented the percent blockade of nerve-evoked twitch responses of the CBCM after a 30 min exposure to the respective toxins. In separate experiments, the reversibility of the neuromuscular blockade produced by IrTx was assessed by washing out the toxin by overflow with fresh Krebs solution at 10 min intervals combined with a slow drip wash over 120 min or by the addition of the anticholinesterase drug neostigmine (10 μM).

Rat phrenic nerve-hemidiaphragm preparations

Male Sprague-Dawely rats were euthanized by exposure to 100% CO$_2$ followed by cervical dislocation, and the rat phrenic nerve-hemidiaphragm (RHD) preparations, with the intact phrenic nerves, were isolated as described previously for the mouse (14). The tissues were mounted in a 6 ml organ bath, essentially under the conditions stated for the CBCM preparation. Indirect nerve stimulation was performed at a frequency of 0.2 Hz in rectangular pulses of 0.2 ms duration at a supramaximal voltage of 7–10 V. The concentration-dependent effects of IrTx (1 and 10 μM) and α-bungarotoxin (0.03–3 μM) on twitch responses of the RHD evoked by electrical field stimulation of the phrenic nerve were studied. Each muscle preparation was exposed only to one dose of

toxin, and at least two replicates were obtained for each concentration, except for concentrations of 1 μM or greater of IrTx, where a single experiment was conducted due to the scarcity of the compound. All animal handling and experimental protocols were conducted in accordance with approved procedures (NNI IACUC TNI-07/1/004).

RESULTS

Protein purification

Irditoxin (IrTx) was purified from venom of *B. irregularis* using gel filtration chromatography, cation exchange HPLC, and final polishing by RP-HPLC (**Fig. 1**). It is an abundant component of the venom and comprises ~10% (peak area) of the total venom protein. Precise mass and homogeneity of native protein were determined by ESI-MS, which showed 6 m/z peaks: 1217.9, 1311.5, 1420.7, 1549.8, 1704.6, and 1893.9, having charges of 14, 13, 12, 11, 10, and 9, respectively, and corresponding to a molecular mass of 17,036.31 ± 0.49 Da (data not shown). No contaminating proteins were found. Reduced toxin (treated with TCEP or DTT) resulted in separation of the subunits (**Fig. 2A**). Covalent linkage between subunits was confirmed by SDS-PAGE; the nonreduced protein appeared as a single ~17 kDa band, and the reduced form was visible as two bands of ~8.5 and 7.5 kDa (Fig. 2B). No free cysteine residues were detected in the native molecule using Ellman's reagent (data not shown). Reduced subunit A has an observed molecular mass of 8379.56 ± 0.20, and subunit B is 8677.79 ± 0.12 (Fig. 2C, D). This covalent association is unique among the 3FTXs, and the toxin contains two subunits linked through a single disulfide bond.

Primary sequence

The two reduced subunits were separated and deblocked with *Pfu* pyroglutamase, and their partial (48%) amino acid sequence was determined by direct NH₂-terminal protein sequencing. The complete sequence was determined by Edman degradation sequencing of overlapping peptide fragments (Supplemental Fig. S1) and through sequencing of clones obtained by constructing a 3′RACE library (**Fig. 3**). Out of 60 clones, 7 and 10 clones exactly matched the amino acid sequences of subunit A and B, respectively. The full-length cDNAs and deduced amino acid sequences of both subunits are shown in Fig. 3. The calculated masses of both the subunits as obtained from cDNA and observed masses from ESI-MS matched exactly. These sequences have been submitted to GenBank (accession numbers DQ304538 and DQ304539 for subunits A and B, respectively). The cDNA encodes for open reading frames of 236 (subunit A) and 230 nucleotides (subunit B). Both termination codons are encoded by TGA, and the polyadenylation signals AUUAAA (less frequent compared with AAUAAA) are located 14 nucleotides upstream of poly-A tail. The deduced amino acid sequence has an additional 34 amino acid residues at the NH₂ terminus when compared with the mature protein. Interestingly, a BLASTX search (National Center for Biotechnology Information) showed hits with insignifi-
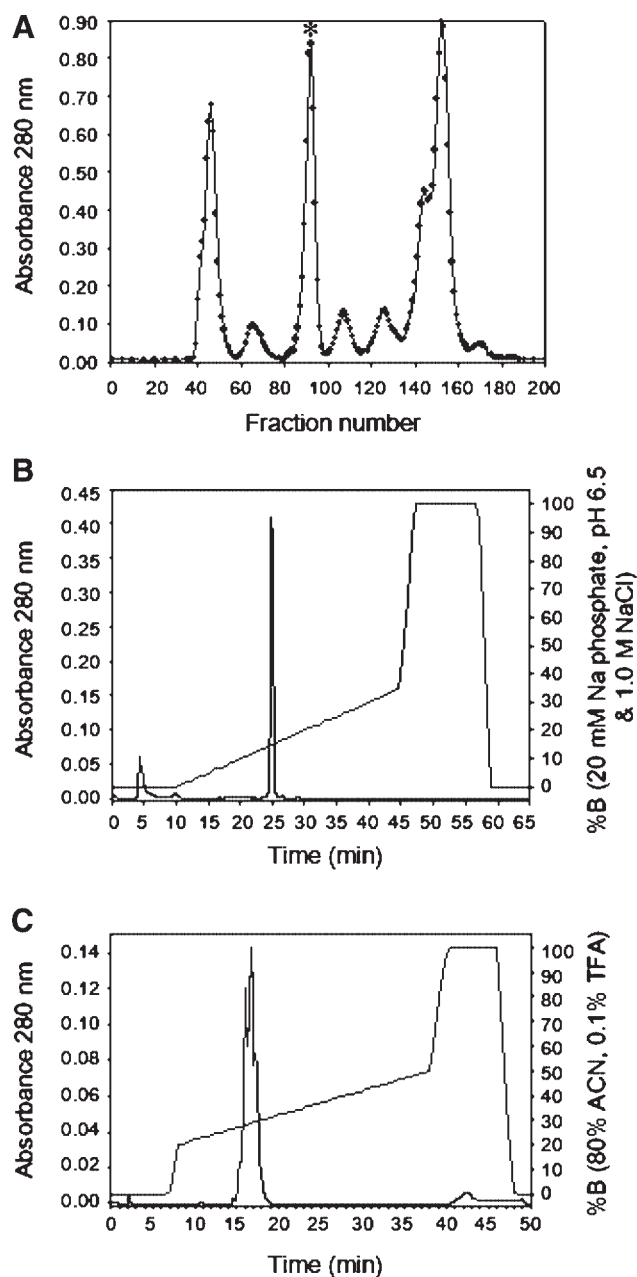
Figure 1. Isolation of IrTx from venom of the brown treesnake (*B. irregularis*). *A*) Chromatogram of 70 mg venom applied to a BioGel P-100 low-pressure column (2.8×90 cm); asterisk indicates peak of interest. *B*) Chromatogram of cation exchange HPLC (BioGel peak III) on a Shodex CM-825 column. *C*) RP-HPLC chromatogram of cation exchange peak on a Jupiter C₄ column; note that IrTx elutes as a heterogeneous peak, even though it is highly purified.

cant E values with any other proteins, and only the conserved signal peptide regions of other 3FTXs matched IrTx sequences.

The toxin subunits A and B have 75 and 77 amino acid residues, respectively. Their NH₂ termini are blocked by a pyroglutamic acid and are considerably longer than most 3FTXs due to the presence of seven additional residues, similar to other colubrid 3FTXs (Fig. 3 and **Fig. 6**). The cysteine pattern in this new toxin is unique. Each subunit contains 11 cysteine
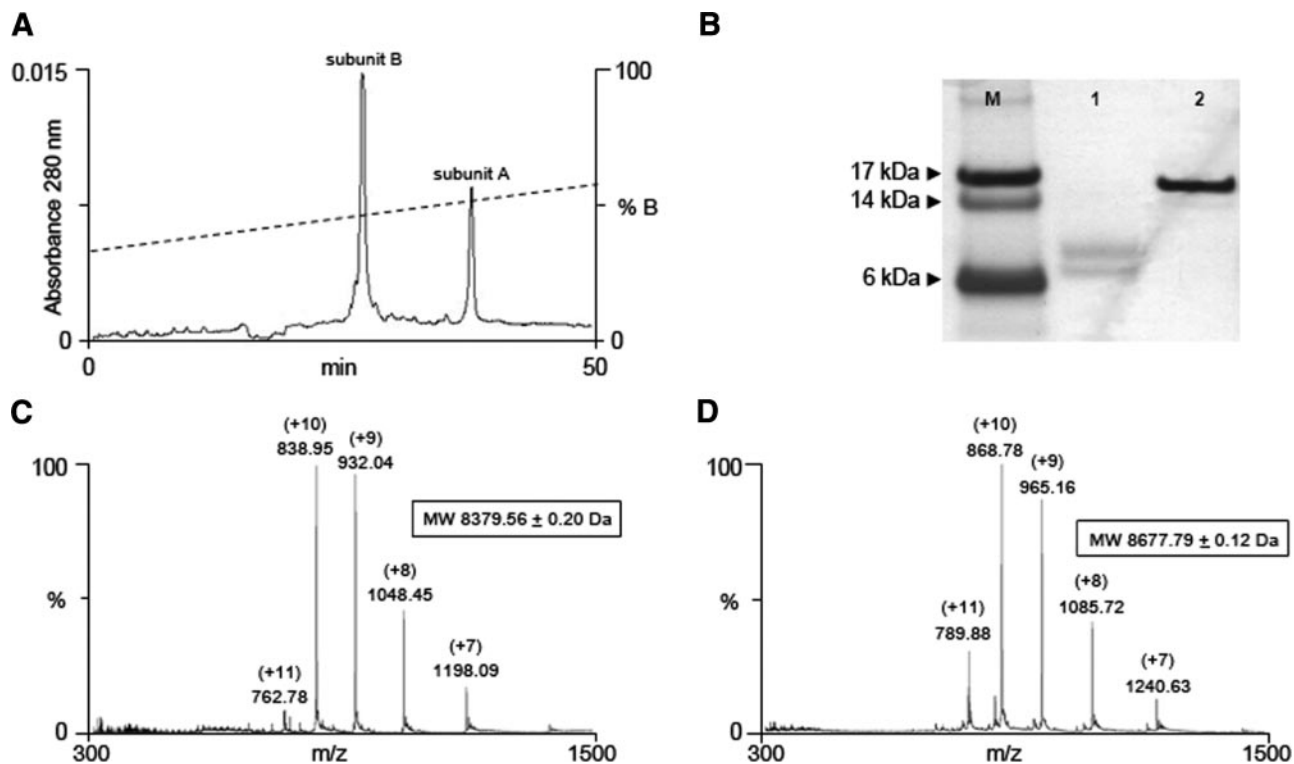
Figure 2. Subunit composition of IrTx. *A*) Separation of subunits. TCEP-treated IrTx was separated *via* RP-HPLC on a C_{18} column with a gradient (dotted line) of 30–60% buffer B (60% acetonitrile in 0.1% TFA) over 50 min. *B*) SDS-PAGE (15% gel, silver staining) of IrTx. M = protein mass standards; 1 = reduced IrTx; 2 = nonreduced IrTx. Native IrTx showed a single ~17 kDa band, whereas reduced sample shows two bands of ~8 kDa each. *C*) ESI-MS spectra of reduced subunit A of IrTx. *D*) ESI-MS spectra of reduced subunit B of IrTx.

residues that participate in the four conserved disulfide bonds as well as a fifth disulfide in the first loop, similar to the nonconventional toxins. The 11th cysteine of subunits A and B is in the tip of the first and second loops, respectively, and forms the disulfide linkage between the two subunits (see structural description below). Thus, this toxin is the first disulfide-linked heterodimeric 3FTX. This new member of the 3FTX family from *B. irregularis* was named "irditoxin" (*B. irregularis* dimeric toxin) to distinguish it from the typical monomeric 3FTXs. The molecular evolutionary relationship of IrTx subunits to other 3FTXs is shown in Supplemental Fig. S2.

General description of the crystal structure

Optimization for crystallization conditions were performed by streak seeding and macroseeding, and the best crystals were used further (Supplemental Fig. S3). Although the crystals diffracted well, initial attempts to solve the structure using molecular replacement techniques were unsuccessful. Therefore, heavy atom derivatives were generated and the structure was then solved using a MIRAS approach. Details of the data collection and processing for all data sets are combined in **Table 1**, and the coordinates of the structure have been deposited in the Protein Data Bank with the code number 2H7Z.

Figure 3. IrTx sequence determination. Pairwise cDNA and amino acid sequence alignments of IrTx subunits. Amino acid differences are highlighted in gray. Arrow shows the start of the mature protein.

Crystals of IrTx contained one heterodimeric molecule per asymmetric unit, with a solvent content of 44.3%.

The IrTx structure (**Fig. 4A**) was refined to 1.5 Å, and for most of the molecule the electron density maps were excellent (Supplemental Fig. S4). However, 17 of the 152 amino acid residues (Gln1A, Ala2A, Val3A, Asn14A, Arg15A, Met16A, Thr17A, Ser18A, Ser19A, Asp20A, Cys21A, Gln1B, Ala2B, Lys3B, Asp41B, Gly42B, and Asn43B) comprising tips of loop I (in subunit A) and loop II (in subunit B; Supplemental Fig. S4B), as well as the NH$_2$ termini of both subunits, were not visible in the electron density map, suggesting high flexibility in these parts of the molecule.

Each subunit of the IrTx heterodimer adopts a β-stranded three-finger fold motif, represented by three adjacent loops extending from the core, which is cross-linked by four conserved disulfide bridges (Fig. 4). The presence of the fifth disulfide bond in the first loop of each subunit demonstrates their similarity to nonconventional 3FTXs (4). Superimposition of the backbones of the two subunits of the IrTx heterodimer illustrates the close structural similarity between them, with a root mean square deviation of only 1.27 Å (Fig. 4B). Most of the observed structural differences are due to the mobility of the tips of loops I and II and the presence of an intersubunit disulfide bond that imparts constraints. Both subunits also show structural similarity to elapid 3FTXs such as short-chain erabutoxin or long-chain α-cobratoxin (Fig. 4C), but several unique

features were observed. The tip of the second loop of both subunits is twisted by the kink created by Pro38A and Pro40B (Fig. 4B). The extraordinarily long NH$_2$ termini, with seven additional residues, are unstructured and show rotational freedom of movement above the core (Fig. 4A), with ample space in the asymmetric unit above the core available to accommodate them.

The monomers of IrTx are placed in a unique diagonal geometry, giving rise to a flattened topology. This arrangement results in two distinct molecular faces. Subunits are related by 2-fold rotation, but the 2-fold axis is not parallel to any crystallographic axes. Loop IIIA, being nearer to loop IB, is inaccessible for receptor interactions as compared with loops IA, IIB, and IIIB, which are free. There is a cluster of hydrophobic interactions between side chains from both monomers (residues: Pro38A, Leu44A, Pro60A, Phe11B, Phe22B, aliphatic Lys23B, Trp48B, and Tyr77B). Loop IIIA interacts with the residues on the outer surface of Loop IB, cushioning dimerization *via* four hydrogen bonds (Supplemental Table S1, with 3.5 Å being taken as an upper limit for a hydrogen bond). There are five additional hydrogen bonds across the dimer interface (Supplemental Table S1). As calculated by GRASP (20), the dimer surface area equals 7616.5 Å^2 (monomer A=4111.99 Å^2; B=4053.59 Å^2). Therefore, 549.08 Å^2 of buried area contributes to the dimer formation. This dimeric interface is distinctly different than that of the homodimeric interface of κ-neurotoxins (see Discussion).

TABLE 1. *Crystallographic data and refinement statistics*

Characteristic	Native	Iodine derivative	Tungstate derivative
		Data set	
Cell parameters (Å)	33.68, 52.11, 45.03	33.89, 51.99, 45.26	33.41, 51.91, 44.86
Cell parameters (deg)	90, 106.29, 90	90, 106.71, 90	90, 105.50, 90
Space group	P2$_1$	P2$_1$	P2$_1$
Data collection			
Resolution range (Å)	52–1.1	99–1.66	43.36–1.7
Wavelength (Å)	1.006768	0.979684	0.979684
Observed reflections	187,362	99,811	203,663
Unique reflections	53,091	33,078	13,978
Completeness (%)	87.0	94.5	100
Overall I/σ (I)	22	15	35.8
R_{sym} (%)[a]	6.9	4.4	6.8
Refinement and quality			
Resolution range (Å)	45–1.5		
R_{work} (reflections)[b]	21.42 (41,024)		
R_{free} (reflections)[c]	23.99 (2092)		
RMSD bond length (Å)	0.011		
RMSD bond angles (deg)	1.77		
Average B-factors (Å^2)			
Main chain	32.0		
Side chains	34.8		
Ramachandran plot			
Most favored regions (%)	79		
Additional allowed regions (%)	19		
Generously allowed regions (%)	1.6		
Disallowed regions (%)	0		

[a]$R_{sym} = \Sigma_{hkl}\Sigma |I_i - |/\Sigma_{hkl}\Sigma |I_i|$, where I_i is the intensity of the ith measurement and I_i- is the mean intensity for that reflection. [b]$R_{work} = \Sigma |F_{obs} - F_{calc}|/\Sigma |F_{obs}|$, where F_{calc} and F_{obs} are the calculated and observed structure factor amplitudes, respectively. [c]$R_{free} =$ as for R_{work} but for 5% of the total reflections chosen at random and omitted from refinement.
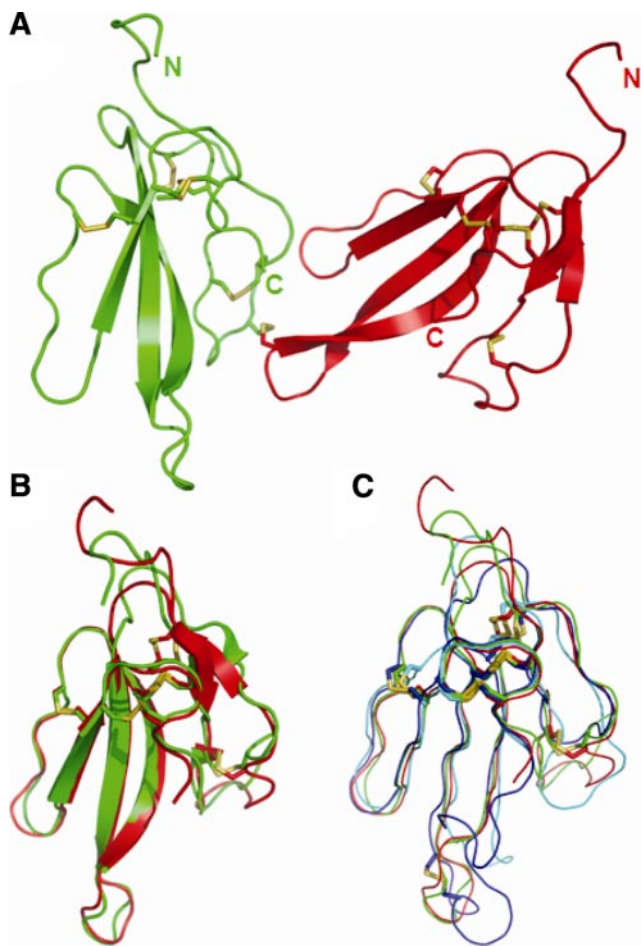
Figure 4. Structural comparison of the subunits of IrTx. *A*) IrTx molecule; note the presence of three β-sheet-defined loops (the "three fingers") in each subunit. *B*) Superimposition of subunits A (red) and B (green) of IrTx. *C*) IrTx subunits (A, red; B, green) superimposed with α-cobratoxin (2CTX, blue) and erabutoxin-b (3EBX, cyan). Cysteine bonds are yellow. Differences within loop regions are clearly seen, but conservation of the three-finger topology is obvious.

Taxon specificity of IrTx

NSA mice showed no effects of IrTx at doses up to 25 μg/g (i.p.). In contrast, *Hemidactylus* geckos showed rapid flaccid paralysis, dyspnea, and increased respiratory rate, and they were unable to maintain adhesion to surfaces at all doses tested, from 0.1 to 10 μg/g. At doses above 1.0 μg/g, death ensued within 10 min to 3 h in a dose-dependent manner ($LD_{50}=0.55$ μg/g). Interestingly, at sublethal doses (0.3 μg/g and below), all animals were immobilized for up to 3 days and then recovered and appeared normal. All chicks injected with lethal doses of IrTx showed rapid onset of inactivity, dyspnea, neck droop, and death ($LD_{50}=0.22$ μg/g); no extended paralysis with survival was seen. The clinical observations seen with IrTx envenomation in lizards and chicks are typical of peripheral nervous system neurotoxicity. Control animals showed no adverse signs.

Species-specific neuromuscular blockade by IrTx

IrTx produced time- and concentration-dependent blockade of nerve-evoked twitch responses in indirectly stimulated CBCM, a typical *in vitro* model of the avian neuromuscular junction (**Fig. 5A**). The contractile responses of the muscle to exogenously applied agonists acetylcholine (300 μM) and carbachol (10 μM) were also completely abolished, whereas responses to exogenous KCl (30 mM) and twitches evoked by direct muscle stimulation were unaffected by IrTx, indicating a blockade of postsynaptic nAChRs and an absence of direct myotoxicity. IrTx ($IC_{50}=11.2\pm2.9$ nM) and α-bungarotoxin (11.4 ± 3.8 nM), a well-characterized postsynaptic α-neurotoxin, showed comparable neuromuscular blocking potency in the CBCM (Fig. 5*B*, *C*). α-Bungarotoxin also produced rapid neuromuscular blockade of the RHD, a typical mammalian model of the neuromuscular junction ($IC_{50}=96\pm19$ nM). In contrast, IrTx was almost three orders of magnitude less effective in the RHD, with 1 μM IrTx producing complete neuromuscular blockade in the CBCM in just 10 min while taking over 200 min to do so in the RHD (Fig. 5*B*, *C*). The neuromuscular blockade produced by IrTx and α-bungarotoxin, in both CBCM and RHD, did not undergo spontaneous reversal (for up to 120 min) and was also not reversed by washing with fresh Krebs solution or the addition of the anticholinesterase drug neostigmine (10 μM; data not shown).

Competitive binding experiments

Because IrTx exhibited neurotoxicity, we examined its effects through competitive binding assays with radiolabeled ligands to nAChRs. Of the three receptors tested in the competitive binding assays, IrTx showed weak binding (at μM concentrations) only to mouse muscle α1βγδ nAChR (Supplemental Fig. S5*B*). No competitive inhibition was observed for two neuronal nAChRs, α3β2 and α7 (Supplemental Fig. S5*A*, *B*, respectively). Further experiments involving homologous receptors from different species are required to understand the species-specific interactions between IrTx and nAChRs or other receptors.

DISCUSSION

In the present study, we have purified and determined the crystal structure of a unique heterodimeric, nonconventional 3FTX from *B. irregularis* venom. With the exception of the structural motif-defining disulfides, IrTx showed very low sequence similarity to other 3FTXs at the cDNA and protein levels. Each monomeric 3FTX subunit possesses an additional 11th cysteine residue, which is involved intersubunit disulfide bond. The structural arrangement of the two monomers is substantially different than that of homodimeric κ-neurotoxins, the only dimeric 3FTX (see below). Functionally, IrTx exhibits potent and taxon-specific postsynaptic neurotoxicity at the avian neuromuscular junction.

Processing and maturation of IrTx subunits

Signal peptides have a short, positively charged NH_2 terminus for penetrability, a central hydrophobic re-
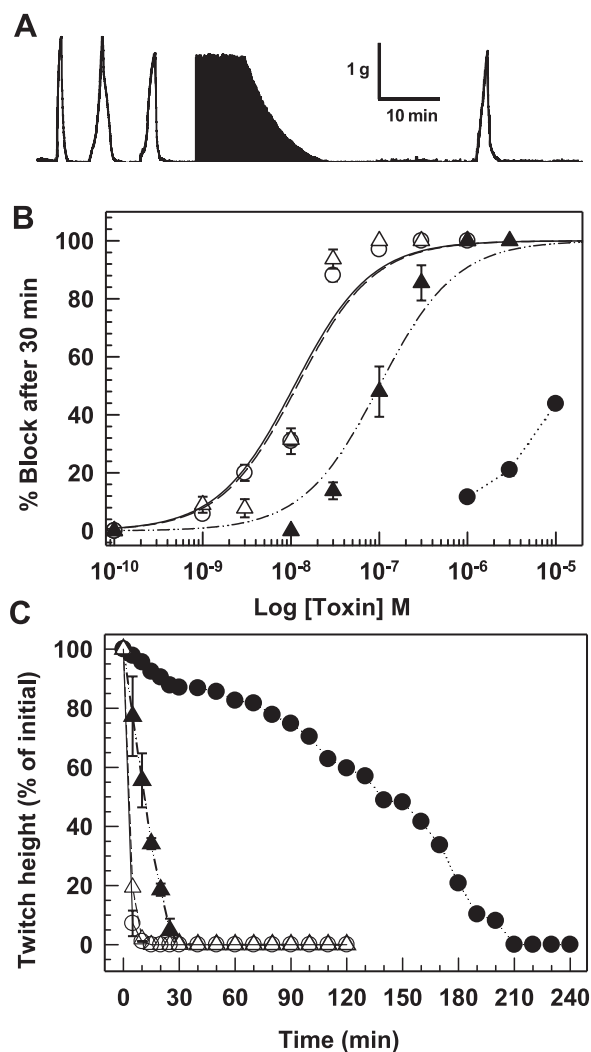
Figure 5. *In vitro* neuromuscular blockade produced by IrTx. *A)* Segment of a trace from a representative experiment demonstrating the postsynaptic blockade produced by IrTx of indirectly stimulated, nerve-evoked twitch responses of the CBCM (0.3 μM). Contractile responses produced by exogenously applied ACh (300 μM), carbachol (CCh; 10 μM), and KCl (30 mM) before and after the addition of the toxin are also shown. *B)* Concentration-response curves for the neuromuscular blockage produced by IrTx (open circle and solid line; solid circle and dotted line) and α-bungarotoxin (open triangle and dashed line; solid triangle and dashed/dotted line) in the CBCM (open symbols) and RHD (solid symbols). Neuromuscular blockade is expressed as % blockade of twitch responses after 30 min of exposure to respective toxins. *C)* Effect of 1 μM IrTx (circles) or 1 μM α-bungarotoxin (triangles) on indirectly-evoked (7–10 V, 0.1 ms, 0.2 Hz) twitches of the isolated CBCM (open symbols) and RHD (solid symbols). Data points in *B* and *C* are means ± SD of at least two experiments, except for concentrations of 1 μM or greater of IrTx, where a single experiment was conducted due to sample limitations.

gion extending across the membrane, and a polar C terminal for signal peptidase cleavage (21). Unlike the largely conserved 21-residue MKTLLLTLVVVTIVCLD-LGYT sequence of all 3FTXs (22, 23), IrTx precursors possess 34 residues (MKTLLLAVAVVAFVCLGSADQL-GLGRQQIDWGKG) at the NH$_2$-terminal side of the

mature subunits (Fig. 3). Although Gly3 and Gly1 residues fit well with Von Heijne's rule, the 34-residue signal peptide is exceptionally long. To date, all other toxin families have only 16- to 27-residue-long signal peptides (24). Moreover, the Signal P software (http://www.cbs.dtu.dk/services/SignalP/; ref. 25) predicts cleavage between Ala16 and Asp15, resulting in a 19-residue signal peptide, which also follows the −3, −1 rule (Gly18 at −3 and Ala16 at −1 positions). This suggests potential propeptide segments (15-residue, 1671 Da) are removed during maturation, which has not been reported in 3FTXs. The maturation process often involves cleavage after dibasic/monobasic (PR) residues. As IrTx subunits do not possess such sites, a novel mechanism may be involved in toxin maturation.

Structurally important residues for the three-finger fold

IrTx shares only ~30% sequence identity with other 3FTXs, and most of this identity is due to conserved disulfide bridges and structurally important residues. Only the monomeric α-colubritoxin (13; isolated from *Coelognathus radiatus*, a colubrid snake) showed higher sequence identity with subunits A and B of IrTx (58 and 55%, respectively). Each subunit possesses four conserved disulfide bridges located in the core region, the reduction of which disturbs the overall conformation and results in total loss of function (26). As expected from the contiguous sequence alignments (Fig. 6), the general fold of each subunit is similar to other 3FTXs. The Dali search algorithm (27) showed structural homology of both subunits of IrTx to erabutoxin-b (*Laticauda semifasciata*), bucandin (*Bungarus candidus*), toxin-b (*Ophiophagus hanna*), and toxin-γ (*Naja nigricollis*). Dali also indicated shared architecture with ectodomains of the transforming growth factor-β superfamily of multifunctional cytokines as well as the complement regulatory protein CD59, both of which are members of the Ly6 superfamily of proteins. Two members of this superfamily, Lynx1 and Lynx2, highly and specifically expressed in the rat brain (28, 29), and SLURP-1 and SLURP-2 from human keratinocytes (30, 31) were found to be novel modulators of neuronal α4β2 and α7 nAChRs. These mammalian proteins are closest in structural similarity to the nonconventional 3FTXs such as candoxin (6), bucandin (32), and IrTx, with the fifth disulfide bond in the first loop. The Lynx and SLURP proteins are therefore considered to be "prototoxins," natural structural and functional mammalian homologues evolutionarily related to snake toxins (29).

In addition to conserved cysteine residues, IrTx subunits have many invariant residues vital for proper folding and three-dimensional structure. The highly conserved Tyr25 (all numbering is according to erabutoxin-a, unless specified otherwise; refs. 33, 34), which stabilizes the antiparallel β-sheet structure (32), has been shown to prevent proper folding of α-cobratoxin in mutational studies (35). IrTx also possesses Tyr37A and Tyr35B, with their side chains in a similar spatial
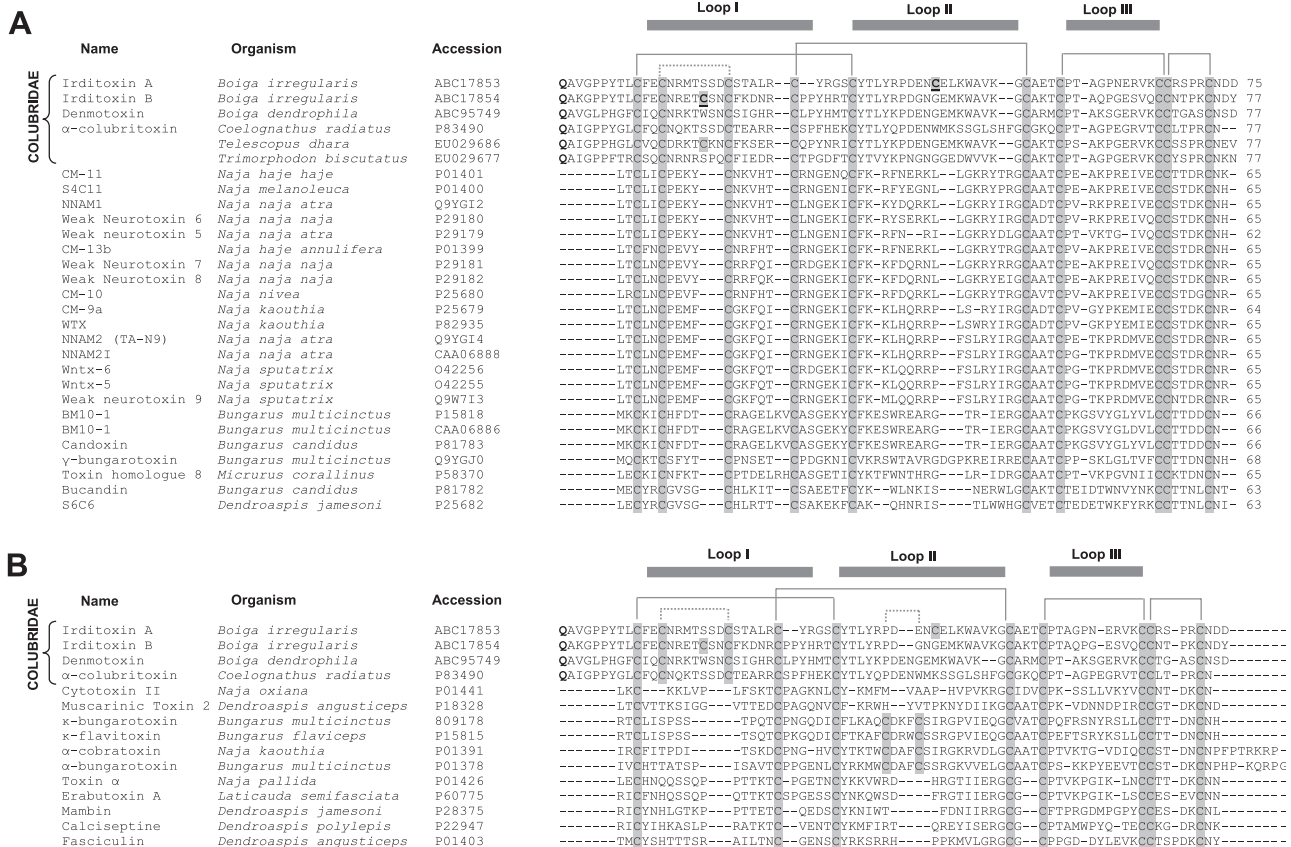
orientation. Gly40, important for maintaining spatial conformation is placed opposite Tyr25 to accommodate its bulky side chain, and equivalent Gly residues (Gly50A and Gly52B) are present in IrTx. Gly42, Pro44, and Pro48 are also involved in the integrity of the three-finger fold (36), and in IrTx Gly42 is replaced by Ala in both chains (Ala52A and Ala54B), whereas Pro44 and Pro48 are both conserved (Pro56A/Pro58B and Pro60A/Pro62B). Arg39, shown to stabilize the native conformation of the protein by salt-bridge formation with the C terminus (34), is replaced by positively charged Lys49A and Lys51B in IrTx, which may interact with Asp74A/Asp75A or Asp76B at the C terminus. However, IrTx lacks a similar electrostatic bond at the N terminus observed in α-cobratoxin, which has Arg2 bridging with Asp60 (34; replaced in IrTx by Pro70A and Pro72B, respectively). The presence of these conserved structurally invariant residues, IrTx retains the overall three-finger fold, despite low sequence identity with other 3FTXs.

Functionally important residues for neurotoxins with a three-finger fold

The functional sites for nAChR binding in short- and long-chain α-neurotoxins have been studied in detail (33, 37, 38). The crystal structures of α-cobratoxin bound to acetylcholine binding protein (39) and of α-bungarotoxin bound to the α1 subunit of the muscle nAChR (40) indicate the critical residues involved in toxin-receptor interactions, specifically the crucial interaction of Arg33/Arg36 (α-cobratoxin/α-bungarotoxin) within the aromatic cage of the binding pocket. Erabutoxin-a and α-cobratoxin interact with *Torpedo* α1βγδ using a common core of residues: *1*) Lys27/Lys23, *2*) Trp29/Trp25, *3*) Asp31/Asp27, *4*) Phe32/Phe29, *5*) Arg33/Arg33, and *6*) Lys47/Lys49. Most of these residues are replaced by unconserved residues in IrTx: *1*) Leu35A/Leu37B, *2*) Arg37A/Arg39B, *3*) Asn41A/Asn43B, *4*) Glu40A/Gly42B, *5*) Asp39A/Asp41B, and *6*) Gly59A/Gln61B. Most importantly, Arg33 is replaced by a negatively charged aspartic acid. Apart from common core residues, erabutoxin-a utilizes specific determinants crucial for *Torpedo* receptor recognition: Gln7, Ser8, Gln10, Ile36, and Glu38. These residues correspond in IrTx to Asn14A/Asn14B, Arg15A/Arg15B, Ser19A/Ser19B, Trp46A/Trp44B, and Val48A/Val46B, respectively. Moreover, due to dimerization, spatial dispositions of the residues involved in receptor interactions are likely altered as compared with those of monomers. These distinct variations suggest that IrTx might have modes of binding to the muscle nAChR different from most curaremimetic 3FTXs.

A

```
                                                              Loop I                    Loop II                   Loop III
        Name              Organism            Accession
  Irditoxin A        Boiga irregularis         ABC17853   QAVGPPYTLCFECNRMTSSDCSTALR--C--YRGSCYTLYRPDENCELKWAVK--GCAETCPT-AGPNERVKCCRSPRCNDD  75
  Irditoxin B        Boiga irregularis         ABC17854   QAKGPPYTLCFECNRETCSNCFKDNR--CPPYHRTCYTLYRPDGNGEMKWAVK--GCAKTCPT-AQPGESVQCCNTPKCNDY  77
  Denmotoxin         Boiga dendrophila         ABC95749   QAVGLPHGFCIQCNRKTWSNCSIGHR-CLPYHMTCYTLYKPDENGEMKWAVK--GCARMCPT-AKSGERVKCCTGASCNSD   77
  α-colubritoxin     Coelognathus radiatus     P83490     QAIGPPYGLCFQCNQKTSSDCTEARR--CSPFHEKCYTLYQPDENWMKSSGLSHFGCGKQCPT-AGPEGRVTCCLTPRCN--  77
                     Telescopus dhara          EU029686   QAIGPPHGLCVQCDRKTCKNCFKSER--CQPYNRICYTLYKPDENGEMKWAVK--GCAKTCPS-AKGPERVKCCSSPRCNEV  77
                     Trimorphodon biscutatus   EU029677   QAIGPPFTRCSQCNRNRSPQCFIEDR--CTPGDFTCYTVYKPNGNGGEDWVVK--GCAKTCPT-AGPGERVKCCYSPRCNKN  77
  CM-11              Naja haje haje            P01401     -------LTCLICPEKY---CNKVHT--CRNGENQCFK-RFNERKL-LGKRYTRGCAATCPE-AKPREIVECCSTDRCNK-   65
  S4C11              Naja melanoleuca          P01400     -------LTCLICPEKY---CNKVHT--CRNGENICFK-RFYEGNL-LGKRYPRGCAATCPE-AKPREIVECCSTDKCNH-   65
  NNAM1              Naja naja atra            Q9YGI2     -------LTCLICPEKY---CNKVHT--CLNGEKICFK-KYDQRKL-LGKRYIRGCADTCPV-RKPREIVECCSTDKCNH-   65
  Weak Neurotoxin 6  Naja naja naja           P29180     -------LTCLICPEKY---CNKVHT--CLNGEKICFK-RYSERKL-LGKRYIRGCADTCPV-RKPREIVQCCSTDKCNH-   65
  Weak neurotoxin 5  Naja naja atra            P29179     -------LTCLICPEKY---CNKVHT--CLNGENICFK-RFN--RI-LGKRYDLGCAATCPT-VKTG-IVQCCSTDKCNH-   62
  CM-13b             Naja haje annulifera      P01399     -------LTCFNCPEVY---CNRFHT--CRNGEKICFK-RFNERKL-LGKRYTRGCAATCPV-AKPREIVECCSTDRCNH-   65
  Weak Neurotoxin 7  Naja naja naja           P29181     -------LTCLNCPEVY---CRRFQI--CRDGEKICFK-KFDQRNL-LGKRYRRGCAATCPE-AKPREIVQCCSTDKCNH-   65
  Weak Neurotoxin 8  Naja naja naja           P29182     -------LTCLNCPEVY---CRRFQK--CRNGEKICFK-KFDQRNL-LGKRYEIGCAATCPE-AKPREIVQCCSTDKCNH-   65
  CM-10              Naja nivea                P25680     -------LRCLNCPEVF---CRRFHT--CRNGEKICFK-RFDQRKL-LGKRYTRGCAVTCPV-AKPREIVECCSTDGCNR-   65
  CM-9a              Naja kaouthia             P25679     -------LTCLNCPEMF---CGKFQI--CRNGEKICFK-KLHQRRP--LS-RYLRGCADTCPV-GYPKEMIECCSTDKCNH-  64
  WTX                Naja kaouthia             P82935     -------LTCLNCPEMF---CGKFQI--CRNGEKICFK-KLHQRRP-LSWRYIRGCADTCPV-GKPYEMIECCSTDKCNR-   65
  NNAM2 (TA-N9)      Naja naja atra            Q9YGI4     -------LTCLNCPEMF---CGKFQI--CRNGEKICFK-KLHQRRP-FSLRYIRGCAATCPE-TKPRDMVECCSTDRCNH-   65
  NNAM2I             Naja naja atra            CAA06888   -------LTCLNCPEMF---CGKFQI--CRNGEKICFK-KLHQRRP-FSLRYIRGCAATCPG-TKPRDMVECCSTDRCNH-   65
  Wntx-6             Naja sputatrix            O42256     -------LTCLNCPEMF---CGKFQT--CRNGEKICFK-KLQQRRP-FSLRYIRGCAATCPG-TKPRDMVECCSTDRCNH-   65
  Wntx-5             Naja sputatrix            O42255     -------LTCLNCPEMF---CGKFQT--CRNGEKICFK-KLQQRRP-FSLRYIRGCAATCPG-TKPRDMVECCSTDRCNH-   65
  Weak neurotoxin 9  Naja sputatrix            Q9W7I3     -------LTCLNCPEMF---CGKFQT--CRNGEKICFK-MLQQRRP-FSLRYIRGCAATCPG-TKPRDMVECCNTDRCNH-   65
  BM10-1             Bungarus multicinctus     P15818     -------MKCKICHFDT--CRAGELKVCASGEKYCFKESWREARG---TR-IERGCAATCPKGSVYGLYVLCCTTDDCN-    66
  BM10-1             Bungarus multicinctus     CAA06886   -------MKCKICHFDT--CRAGELKVCASGEKYCFKESWREARG---TR-IERGCAATCPKGSVYGLDVLCCTTDDCN-    66
  Candoxin           Bungarus candidus         P81783     -------MKCKICNFDT--CRAGELKVCASGEKYCFKESWREARG---TR-IERGCAATCPKGSVYGLYVLCCTTDDCN-    66
  γ-bungarotoxin     Bungarus multicinctus     Q9YGJ0     -------MQCKTCSFYT---CPNSET--CPDGKNICVKRSWTAVRGDGPKREIRRECAATCPP-SKLGLTVFCCTTDNCNH-  68
  Toxin homologue 8  Micrurus corallinus       P58370     -------LECKICNFKT---CPTDELRHCASGETICYKTFWNTHRG---LR-IDRGCAATCPT-VKPGVNIICCSTDKCN-   65
  Bucandin           Bungarus candidus         P81782     -------MECYRCGVSG---CHLKIT--CSAEETFCYK--WLNKIS----NERWLGCAKTCTEIDTWNVYNKCCTNLCNT-   63
  S6C6               Dendroaspis jamesoni      P25682     -------LECYRCGVSG---CHLRTT--CSAKEKFCAK--QHNRIS----TLWWHGCVETCTEDETWKFYRKCCTNLCNI-   63
```

B

```
                                                              Loop I                  Loop II                 Loop III
        Name              Organism            Accession
  Irditoxin A        Boiga irregularis         ABC17853   QAVGPPYTLCFECNRMTSSDCSTALRC--YRGSCYTLYRPD--ENCELKWAVKGCAETCPTAGPN-ERVKCCRS-PRCNDD-------
  Irditoxin B        Boiga irregularis         ABC17854   QAKGPPYTLCFECNRETCSNCFKDNRCPPYHRTCYTLYRPDGNGEMKWAVKGCAKTCPTAQPG-ESVQCCNY-PKCNDY-------
  Denmotoxin         Boiga dendrophila         ABC95749   QAVGLPHGFCIQCNRKTWSNCSIGHRCLPYHMTCYTLYKPDENGEMKWAVK--GCARMCPTAKSGERVKCCTG-ASCNSD-------
  α-colubritoxin     Coelognathus radiatus     P83490     QAIGPPYGLCFQCNQKTSSDCTEARRCSPFHEKCYTLYQPDENWMKSSGLSHFGCGKQCPTAGPE-GRVTCCLT-PRCN---------
  Cytotoxin II       Naja oxiana               P01441     -------LKC---KKLVP---LFSKTCPAGKNLCY-KMFM--VAAP-HVPVKRGCIDVCPK-SSLLVKYVCCNT-DKCN---------
  Muscarinic Toxin 2 Dendroaspis angusticeps   P18328     -LTCVTTKSIGG---VTTEDCPAGQNVCF-KRWH--YVTPKNYDIIKGCAATCPK-VDNNDPIRCCGT-DKCND---------
  κ-bungarotoxin     Bungarus multicinctus     809178     -------RTCLISPSS------TPQTCPNGQDICF-KLKAQCDKFCSIRGPVIEQGCVATCPQFRSNYRSLLCCTT-DNCNH------
  κ-flavitoxin       Bungarus flaviceps        P15815     -------RTCLISPSS------TSQTCPKGQDICFTKAFCDRWCSSRGPVIEQGCAATCPEFTSRYKSLLCCTT-DNCNH------
  α-cobratoxin       Naja kaouthia             P01391     -------IRCFITPDI------TSKDCPNG-HVCYTKTWCDAFCSIRGKRVDLGCAATCPTVKTG-VDIQCCST-DNCNPFPTRKRP-
  α-bungarotoxin     Bungarus multicinctus     P01378     -------IVCHTTATSP----ISAVTCPPGENLCYRKMWCDAFCSSRGKVVELGCAATCPS-KKPYEEVTCCST-DKCNPHP-KQRPG
  Toxin α            Naja pallida              P01426     -------LECHNQQSSQP---PTTKTC-PGETNCYKKVWRD----HRGTIIERGCG--CPTVKPGIK-LNCCTT-DKCNN--------
  Erabutoxin A       Laticauda semifasciata    P60775     -------RICFNHQSSQP---QTTKTCSPGESSCYNKQWSD----FRGTIIERGCG--CPTVKPGIK-LSCCES-EVCNN--------
  Mambin             Dendroaspis jamesoni      P28375     -------RICYNHLGTKP---PTTETC--QEDSCYKNIWT------FDNIIRRGCG--CFTPRGDMPGPYCCES-DKCNL--------
  Calciseptine       Dendroaspis polylepis     P22947     -------RICYIHKASLP---RATKTC--VENTCYKMFIRT----QREYISERGCG--CPTAMWPYQ-TECCKG-DRCNK--------
  Fasciculin         Dendroaspis angusticeps   P01403     -------TMCYSHTTTSR---AILTNC--GENSCYRKSRRH----PPKMVLGRGCG--CPPGD-DYLEVKCCSTPDKCNY--------
```

Figure 6. Multiple sequence alignments of IrTx subunits with other. *A*) Nonconventional three-fingered toxins. *B*) Conventional three-fingered toxins. Toxin names are followed by species names and the SwissProt accession number. The five disulfide bridges and loop regions are outlined. Cysteines are marked in gray. The two additional cysteines of IrTx that form the dimer are underlined.

Structural and functional comparison with κ-neurotoxins

The monomers of κ-neurotoxins are arranged with a 2-fold symmetry axis and ∼180° rotation in such a way that the β-strands in the third loop of both subunits oppose each other, forming an antiparallel β-sheet, while those of IrTx have the 2-fold symmetry axis but are placed in a diagonal geometry. Moreover, the dimer interface in κ-neurotoxins is formed by main-chain and side-chain hydrogen bonds, together with Van der Waal's interactions of Phe49 and Leu57 (41; **Fig. 7**). In IrTx, although there is a hydrophobic cluster in the dimer interface, dimerization is due to covalently linked cysteines. Functionally, κ-neurotoxins bind with high affinity to neuronal α3β2 and α4β2 receptors (42), whereas IrTx does not. IrTx appears to be pharmacologically more closely related to short-chain α-neurotoxins such as erabutoxin-a and -b, as it shows high affinity toward muscle but not α3β2 nAChRs (as κ-neurotoxins) or neuronal α7 nAChRs (as long-chain α-neurotoxins; Supplemental Fig. S5).

Species-specific neurotoxicity of IrTx

IrTx induced rapid paralysis in lizards and chicks and, in lethal doses, produced death by respiratory paralysis, indicating a peripheral, postsynaptic neurotoxic effect. Its bioactivity was taxon specific, lethal to lizards and chicks with LD_{50} values of 0.55 and 0.22 μg/g, respectively, but nontoxic to mice at doses up to 25 μg/g. In *in vitro* studies, the dimeric IrTx exhibited potent postsynaptic neuromuscular blockade of avian skeletal muscle, with an efficacy nearly identical with the prototypical, monomeric α-bungarotoxin (IC_{50}∼11 nM), but was three orders of magnitude less effective on mammalian motor endplate preparations. In contrast, α-bungarotoxin produced potent blockade of both chick and rat (IC_{50}=96 nM) skeletal muscle. This differential binding of IrTx to the muscle-type nAChRs of the two species strongly supports the observed taxon-specific toxicity. Furthermore, in radioligand competitive binding studies, IrTx showed weak binding to mouse muscle but not to α7 and α3β2 nAChRs, exhibiting the pharmacological profile of short-chain α-neurotoxins that bind only to the muscle type of nAChRs.

Prey preference is known to be an important determinant of venom composition in many snakes (43, 44), and the presence of prey-specific components has been documented in colubrid venoms (45), including *B. irregularis* (17). In some instances, species-specific susceptibility and resistance to predator venoms (mongoose, cobra) result from substitution of several amino acid residues or *N*-glycosylation of muscle nAChRs (46). Possible explanations for IrTx specificity include subtle but significant sequence variation among nAChR subunits across species, different binding sites in the nAChR for IrTx, and an as yet uncharacterized primary molecular target (such as the α10 nAChR), which is present in lizards and chicks but not in mice. The presence of this potent taxon-specific neurotoxin in *B. irregularis* venom demonstrates that the low toxicity of this species' venom toward mammals, including humans, is not because toxins are absent but because their effects are targeting natural nonmammalian prey.

Figure 7. Comparison of the subunit arrangements between IrTx and κ-toxins. *A*) Heterodimeric covalently linked IrTx. *B*) Homodimeric κ-bungarotoxin [1KBA] held by hydrogen bonds and Van der Waals interactions. *C, D*) Schematic representation of arrangements of subunits in IrTx (*C*) and κ-bungarotoxin (*D*).
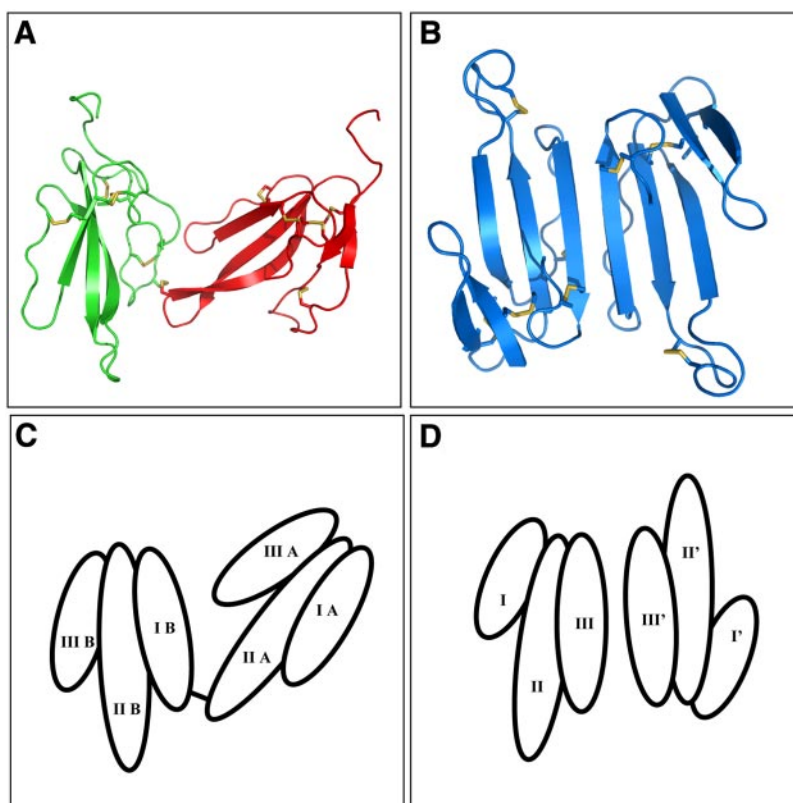
Colubrid *vs* elapid 3FTXs

Several unique features characteristic of colubrid 3FTXs stand out. The first cysteine residue is located at position 10, not 3, and the N terminus is elongated in comparison to elapid and hydrophiid 3FTXs. Colubrid 3FTXs contain a pyroglutamic acid residue blocking the NH$_2$ terminus, a feature not observed in any other 3FTX. We recently showed the presence of glutamyl cyclase in the venom glands of *B. irregularis* (47), and this enzyme is likely involved in post-translational processing of these toxins. Colubrid 3FTX sequences show conserved proline residues, which introduce twists into the second loop, with two negatively charged residues (Glu and Asn) at the tip of it. Although the 10th cysteine backbone in colubrid 3FTXs is similar to elapid nonconventional toxins, each IrTx subunit has an additional 11th cysteine (involved in intermolecular disulfide bridge formation) at the tip of the first or second loop. Short conserved sequence motifs are also observed: CYTLY and CPTA are seen in all colubrid toxins, and the KWAVKGC motif is prominent in 3FTXs isolated from the *Boiga* species (see Fig. 6).

Crystal structures of colubrid 3FTXs show a strong resemblance to elapid 3FTX structures. However, minor differences, such as the twist of second loop and the unstructured, flexible NH$_2$ terminus, are to be noted because they may have functional significance. Moreover, dimeric colubrid toxins have very unique spatial arrangements of their subunits and surface area when compared with monomeric 3FTXs and κ-neurotoxins. Functionally, colubrid 3FTXs often show potent postsynaptic neurotoxicity, with denmotoxin (14) and IrTx being highly species specific.

During the final preparation of this study, a report appeared (48) that described dimeric 3FTXs from an elapid snake (*Naja kaouthia*). Based on partial sequence and mass spectrometry data, these dimers appear to be composed of several well-characterized monomeric toxins from the same venom (α-cobratoxin and several cytotoxins). All these elapid dimers retain their ability to block α7, and the α-cobratoxin dimer, in contrast to the monomer, also blocks α3β2 nAChRs, whereas IrTx does not bind to either receptor. Unlike IrTx, the elapid monomers involved do not have the additional 11th (or 9th) cysteine residues, and at least two interchain disulfide bonds are involved in their dimerization. Further, these interchain disulfides are located in the hydrophobic core (as opposed to the interchain disulfide at the tip of IrTx fingers). In addition, the elapid dimers are very minor venom constituents (total <0.1%), whereas IrTx is a major component of brown treesnake venom (>10%), and hence have significant differential implications to the pharmacological properties of the respective whole venoms.

CONCLUSIONS

We have purified and characterized the structure and pharmacology of a novel, covalently linked heterodimeric three-finger toxin, IrTx that shows taxon-specific toxic-

ity. In addition to monomeric forms, these covalently linked heterodimers of nonconventional three-finger toxins appear to be abundant in colubrid snake venoms (49) and constitute a nonhomogeneous and poorly characterized group of venom peptides. Like elapid neurotoxins, these dimeric toxins may interact with a great diversity of molecular targets. Colubrid three-finger toxins are clearly a very useful source of novel neurobiology probes and therapeutic leads, and we believe they contain tremendous pharmacological potential as well. FJ

REFERENCES

1. Lewis, R. J., and Garcia, M. L. (2003) Therapeutic potential of venom peptides. *Nat. Rev. Drug Discov.* **2,** 790–802
2. Kini, R. M. (2002) Molecular molds with multiple missions: functional sites in three-finger toxins. *Clin. Exp. Pharmacol. Physiol.* **29,** 815–822
3. Fry, B. G., Wuster, W., Kini, R. M., Brusic, V., Khan, A., Venkataraman, D., and Rooney, A. P. (2003) Molecular evolution of elapid snake venom three finger toxins. *J. Mol. Evol.* **57,** 110–129
4. Nirthanan, S., Gopalakrishnakone, P., Gwee, M. C., Khoo, H. E., and Kini, R. M. (2003) Non-conventional toxins from elapid venoms. *Toxicon* **41,** 397–407
5. Poh, S. L., Mourier, G., Thai, R., Armugam, A., Molgo, J., Servent, D., Jeyaseelan, K., and Menez, A. (2002) A synthetic weak neurotoxin binds with low affinity to Torpedo and chicken α7 nicotinic acetylcholine receptors. *Eur. J. Biochem.* **269,** 4247–4256
6. Nirthanan, S., Charpantier, E., Gopalakrishnakone, P., Gwee, M. C., Khoo, H. E., Cheah, L. S., Bertrand, D., and Kini, R. M. (2002) Candoxin, a novel toxin from *Bungarus candidus*, is a reversible antagonist of muscle (αβγδ) but a poorly reversible antagonist of neuronal α7 nicotinic acetylcholine receptors. *J. Biol. Chem.* **277,** 17811–17820
7. Ricciardi, A., Le Du, M. H., Khayati, M., Dajas, F., Boulain, J. C., Menez, A., and Ducancel, F. (2000) Do structural deviations between toxins adopting the same fold reflect functional differences? *J. Biol. Chem.* **275,** 18302–18310
8. Ohno, M., Menez, R., Ogawa, T., Danse, J. M., Shimohigashi, Y., Fromen, C., Ducancel, F., Zinn-Justin, S., Le Du, M. H., Boulain, J. C., Tamiya, T., and Menez, A. (1998) Molecular evolution of snake toxins: is the functional diversity of snake toxins associated with a mechanism of accelerated evolution? *Prog. Nucleic Acids Res. Mol. Biol.* **59,** 307–364
9. Banerjee, Y., Mizuguchi, J., Iwanaga, S., and Kini, R. M. (2005) Hemextin AB complex-a unique anticoagulant protein complex from *Hemachatus haemachatus* (African Ringhals cobra) venom that inhibits clot initiation and factor VIIa activity. *J. Biol. Chem.* **280,** 42601–42611
10. Rajagopalan, N., Pung, Y. F., Zhu, Y. Z., Wong, P. T., Kumar, P. P., and Kini, R. M. (2007) β-Cardiotoxin: a new three-finger toxin from *Ophiophagus hannah* (king cobra) venom with beta-blocker activity. *FASEB J.* **21,** 3685–3695

11. Junqueira-de-Azevedo, I. L., Ching, A. T., Carvalho, E., Faria, F., Nishiyama, M. Y., Jr., Ho, P. L., and Diniz, M. R. (2006) *Lachesis muta* (*Viperidae*) cDNAs reveal diverging pit viper molecules and scaffolds typical of cobra (*Elapidae*) venoms: implications for snake toxin repertoire evolution. *Genetics* **173,** 877–889

12. Pahari, S., Mackessy, S. P., and Kini, R. M. (2007) The venom gland transcriptome of the desert massasauga rattlesnake (*Sistrurus catenatus edwardsii*): towards an understanding of venom composition among advanced snakes (superfamily *Colubroidea*). *BMC Mol. Biol.* **8,** 115

13. Fry, B. G., Lumsden, N. G., Wuster, W., Wickramaratna, J. C., Hodgson, W. C., and Kini, R. M. (2003) Isolation of a neurotoxin (α-colubritoxin) from a nonvenomous colubrid: evidence for early origin of venom in snakes. *J. Mol. Evol.* **57,** 446–452

14. Pawlak, J., Mackessy, S. P., Fry, B. G., Bhatia, M., Mourier, G., Fruchart-Gaillard, C., Servent, D., Menez, R., Stura, E., Menez, A., and Kini, R. M. (2006) Denmotoxin, a three-finger toxin from the colubrid snake *Boiga dendrophila* (mangrove catsnake) with bird-specific activity. *J. Biol. Chem.* **281,** 29030–29041

15. Fry, B. G., Scheib, H., van der Weerd, L., Young, B., McNaughtan, J., Ramjan, S. F., Vidal, N., Poelmann, R. E., and Norman, J. A. (2008) Evolution of an arsenal: structural and functional diversification of the venom system in the advanced snakes (*Caenophidia*). *Mol. Cell Proteomics* **7,** 215–246

16. Hill, R. E., and Mackessy, S. P. (2000) Characterization of venom (Duvernoy's secretion) from twelve species of colubrid snakes and partial sequence of four venom proteins. *Toxicon* **38,** 1663–1687

17. Mackessy, S. P., Sixberry, N. M., Heyborne, W. H., and Fritts, T. (2006) Venom of the brown treesnake, *Boiga irregularis*: ontogenetic shifts and taxa-specific toxicity. *Toxicon* **47,** 537–548

18. Hill, R. E., and Mackessy, S. P. (1997) Venom yields from several species of colubrid snakes and differential effects of ketamine. *Toxicon* **35,** 671–678

19. Otwinowski, Z., and Minor, W. (1997) Macromolecular crystallography, part A: processing of X-ray diffraction data collected in oscillation mode. In *Methods of Enzymology* (Carter, C. W., Jr., and Sweet, R. M., eds) pp. 307–326, Academic Press, New York, NY, USA

20. Nicholls, A., Bharadwaj, R., and Honig, B. (1993) GRASP: Graphical representation and analysis of surface properties. *Biophys. J.* **64,** A166

21. Von Heijne, G. (1986) A new method for predicting signal sequence cleavage sites. *Nucleic Acids Res.* **14,** 4683–4690

22. Tamiya, T., Lamouroux, A., Julien, J. F., Grima, B., Mallet, J., Fromageot, P., and Menez, A. (1985) Cloning and sequence analysis of the cDNA encoding a snake neurotoxin precursor. *Biochimie* **67,** 185–189

23. Afifiyan, F., Armugam, A., Gopalakrishnakone, P., Tan, N. H., Tan, C. H., and Jeyaseelan, K. (1998) Four new postsynaptic neurotoxins from *Naja naja sputatrix* venom: cDNA cloning, protein expression, and phylogenetic analysis. *Toxicon* **36,** 1871–1885

24. Smith, L. A. (1990) Cloning, characterization, and expression of animal toxin genes for vaccine development. *J. Toxicol. Toxin Rev.* **9,** 243–283

25. Bendtsen, J. D., Nielsen, H., von Heijne, G., and Brunak, S. (2004) Improved prediction of signal peptides: SignalP 3.0. *J. Mol. Biol.* **340,** 783–795

26. Menez, A., Bouet, F., Guschlbauer, W., and Fromageot, P. (1980) Refolding of reduced short neurotoxins: circular dichroism analysis. *Biochemistry* **19,** 4166–4172

27. Holm, L., and Sander, C. (1995) Dali: a network tool for protein structure comparison. *Trends Biochem. Sci.* **20,** 478–480

28. Miwa, J. M., Ibanez-Tallon, I., Crabtree, G. W., Sanchez, R., Sali, A., Role, L. W., and Heintz, N. (1999) Lynx1, an endogenous toxin-like modulator of nicotinic acetylcholine receptors in the mammalian CNS. *Neuron* **23,** 105–114

29. Ibanez-Tallon, I., Miwa, J. M., Wang, H. L., Adams, N. C., Crabtree, G. W., Sine, S. M., and Heintz, N. (2002) Novel modulation of neuronal nicotinic acetylcholine receptors by association with the endogenous prototoxin lynx1. *Neuron* **33,** 893–903

30. Chimienti, F., Hogg, R. C., Plantard, L., Lehmann, C., Brakch, N., Fischer, J., Huber, M., Bertrand, D., and Hohl, D. (2003) Identification of SLURP-1 as an epidermal neuromodulator explains the clinical phenotype of Mal de Meleda. *Hum. Mol. Genet.* **12,** 3017–3024

31. Arredondo, J., Chernyavsky, A. I., Jolkovsky, D. L., Webber, R. J., and Grando, S. A. (2006) SLURP-2: A novel cholinergic signaling peptide in human mucocutaneous epithelium. *J. Cell. Physiol.* **208,** 238–245

32. Torres, A. M., Kini, R. M., Selvanayagam, N., and Kuchel, P. W. (2001) NMR structure of bucandin, a neurotoxin from the venom of the Malayan krait (*Bungarus candidus*). *Biochem. J.* **360,** 539–548

33. Dufton, M. J., and Hider, R. C. (1988) Structure and pharmacology of elapid cytotoxins. *Pharmacol. Ther.* **36,** 1–40

34. Endo, T., and Tamiya, N. (1991) Structure-function relationships of postsynaptic neurotoxins from the snake venoms. In *Snake Toxins* (Harvey, A. L., ed) pp. 165–222, Pergamon, Oxford, England

35. Antil, S., Servent, D., and Menez, A. (1999) Variability among the sites by which curaremimetic toxins bind to torpedo acetylcholine receptor, as revealed by identification of the functional residues of α-cobratoxin. *J. Biol. Chem.* **274,** 34851–34858

36. Menez, A., Boulain, J. C., Bouet, F., Couderc, J., Faure, G., Rousselet, A., Tremeau, O., Gatineau, E., and Fromageot, P. (1984) On the molecular mechanisms of neutralization of a cobra neurotoxin by specific antibodies. *J. Physiol.* **79,** 196–206

37. Fruchart-Gaillard, C., Gilquin, B., Antil-Delbeke, S., Le Novere, N., Tamiya, T., Corringer, P. J., Changeux, J. P., Menez, A., and Servent, D. (2002) Experimentally based model of a complex between a snake toxin and the α7 nicotinic receptor. *Proc. Natl. Acad. Sci. U. S. A.* **99,** 3216–3221

38. Teixeira-Clerc, F., Menez, A., and Kessler, P. (2002) How do short neurotoxins bind to a muscular-type nicotinic acetylcholine receptor? *J. Biol. Chem.* **277,** 25741–25747

39. Bourne, Y., Talley, T. T., Hansen, S. B., Taylor, P., and Marchot, P. (2005) Crystal structure of a Cbtx-AChBP complex reveals essential interactions between snake α-neurotoxins and nicotinic receptors. *EMBO J.* **24,** 1512–1522

40. Dellisanti, C. D., Yao, Y., Stroud, J. C., Wang, Z. Z., and Chen, L. (2007) Crystal structure of the extracellular domain of nAChR α1 bound to α-bungarotoxin at 1.94 Å resolution. *Nat. Neurosci.* **10,** 953–962

41. Dewan, J. C., Grant, G. A., and Sacchettini, J. C. (1994) Crystal structure of κ-bungarotoxin at 2.3 Å resolution. *Biochemistry* **33,** 13147–13154

42. Chiappinelli, V. A., Weaver, W. R., McLane, K. E., Conti-Fine, B. M., Fiordalisi, J. J., and Grant, G.A. (1996) Binding of native κ-neurotoxins and site-directed mutants to nicotinic acetylcholine receptors. *Toxicon* **34,** 1243–1256

43. Daltry, J. C., Wuster, W., and Thorpe, R. S. (1996) Diet and snake venom evolution. *Nature* **379,** 537–540

44. Pahari, S., Bickford, D., Fry, B. G., and Kini, R. M. (2007) Expression pattern of three-finger toxin and phospholipase A2 genes in the venom glands of two sea snakes, *Lapemis curtus* and *Acalyptophis peronii*: comparison of evolution of these toxins in land snakes, sea kraits and sea snakes. *BMC Evol. Biol.* **7,** 175

45. Mackessy, S. P. (2002) Biochemistry and pharmacology of colubrid snake venoms. *J. Toxicol. Toxin. Rev.* **21,** 43–83

46. Barchan, D., Kachalsky, S., Neumann, D., Vogel, Z., Ovadia, M., Kochva, E., and Fuchs, S. (1992) How the mongoose can fight the snake: the binding site of the mongoose acetylcholine receptor. *Proc. Natl. Acad. Sci. U. S. A.* **89,** 7717–7721

47. Pawlak, J., and Kini, M. R. (2006) Snake venom glutaminyl cyclase. *Toxicon* **48,** 278–286

48. Osipov, A. V., Kasheverov, I. E., Makarova, Y. V., Starkov, V. G., Vorontsova, O. V., Ziganshin, R. Kh., Andreeva, T. V., Serebryakova, M. V., Benoit, A., Hogg, R. C., Bertrand, D., Tsetlin, V. I., and Utkin, Y. N. (2008) Naturally occurring disulfide-bound dimers of three-fingered toxins - a paradigm for biological activity diversification. *J. Biol. Chem.* **283,** 14571–14580

49. Fry, B. G., Wuster, W., Ryan Ramjan, S. F., Jackson, T., Martelli, P., and Kini, R. M. (2003b) Analysis of *Colubroidea* snake venoms by liquid chromatography with mass spectrometry: evolutionary and toxinological implications. *Rapid Commun. Mass. Spectrom.* **17,** 2047–2062